Nanoscale

PAPER

View Article Online
View Journal | View Issue

Cite this: *Nanoscale*, 2020, **12**, 895

Writing chemical patterns using electrospun fibers as nanoscale inkpots for directed assembly of colloidal nanocrystals†

N. Burak Kiremitler,[a,b] Ilker Torun,[a,b] Yemliha Altintas,[c] Javier Patarroyo,[d] Hilmi Volkan Demir,[*e,f,i] Victor F. Puntes,[*d,g] Evren Mutlugun[*e,h] and M. Serdar Onses[*a,b,e]

Received 18th September 2019,
Accepted 17th November 2019

DOI: 10.1039/c9nr08056b

rsc.li/nanoscale

Applications that range from electronics to biotechnology will greatly benefit from low-cost, scalable and multiplex fabrication of spatially defined arrays of colloidal inorganic nanocrystals. In this work, we present a novel additive patterning approach based on the use of electrospun nanofibers (NFs) as inkpots for end-functional polymers. The localized grafting of end-functional polymers from spatially defined nanofibers results in covalently bound chemical patterns. The main factors that determine the width of the nanopatterns are the diameter of the NF and the extent of spreading during the thermal annealing process. Lowering the surface energy of the substrates *via* silanization and a proper choice of the grafting conditions enable the fabrication of nanoscale patterns over centimeter length scales. The fabricated patterns of end-grafted polymers serve as the templates for spatially defined assembly of colloidal metal and metal oxide nanocrystals of varying sizes (15 to 100 nm), shapes (spherical, cube, rod), and compositions (Au, Ag, Pt, TiO_2), as well as semiconductor quantum dots, including the assembly of semiconductor nanoplatelets.

Introduction

Colloidal nanocrystals (NCs), nanoscopic inorganic particles that are dispersed in a solvent, have been extensively studied over the past three decades due to their size and shape dependent fascinating properties that are distinct from bulk materials.[1,2] These intrinsic properties make them promising materials as fundamental building blocks for a broad range of emerging applications in photonics,[3,4] plasmonics,[4–7] electronics,[7–10] and catalysis.[11–16] Nowadays, synthesis techniques of NCs (metal, metal oxide, semiconductor) are robust and well known to prepare NCs with the desired composition, shape and size.[17–19] Most applications of inorganic NCs in devices require a spatially defined assembly of these nanomaterials rather than their colloidal counterparts. Indeed, materials built with nanocrystals are of special significance due to their potential diversity in composition, structure and properties, with access to multiple length scales.[20] For example, layers of assembled NCs termed the "nanocrystal solid" exhibit superior properties compared with thin films and bulk materials[21] or the combination of different magnetic NCs in the same solid leads to new magnetic behavior.[22]

Spatially defined assembly of NCs on solid substrates is a fascinating process that allows for tuning the collective properties of NCs and their integration into functional devices.[23] Typically, chemical and topographic patterns have been used for the directed assembly of NCs.[20–25] The assembly of these NCs on patterned surfaces can be realized *via* various interactions such as electrostatic, magnetic, chemical, capillary

[a]*ERNAM – Erciyes University Nanotechnology Application and Research Center, Kayseri, 38039, Turkey. E-mail: onses@erciyes.edu.tr*
[b]*Department of Materials Science and Engineering, Erciyes University, Kayseri, 38039, Turkey*
[c]*Department of Materials Science and Nanotechnology Engineering, Abdullah Gul University, Kayseri, 38080, Turkey*
[d]*Catalan Institute of Nanoscience and Nanotechnology (ICN2), CSIC and BIST, Campus UAB, Bellaterra, 08193 Barcelona, Spain. E-mail: victor.puntes@icn2.cat*
[e]*UNAM – Institute of Materials Science and Nanotechnology, Bilkent University, Ankara, 06800, Turkey. E-mail: volkan@bilkent.edu.tr, evren.mutlugun@agu.edu.tr*
[f]*Luminous! Center of Excellence for Semiconductor Lighting and Displays, School of Electrical and Electronic Engineering, School of Physical and Materials Sciences, School of Materials Science and Nanotechnology, Nanyang Technological University, 639798, Singapore*
[g]*Institució Catalana de Recerca i Estudis Avançats (ICREA), 08010 Barcelona, Spain*
[h]*Department of Electrical and Electronics Engineering, Abdullah Gul University, Kayseri, 38080, Turkey*
[i]*Department of Electrical and Electronics Engineering, Department of Physics, Bilkent University, Ankara 06800, Turkey*

†Electronic supplementary information (ESI) available: Additional experimental details, AFM, SEM and TEM images, schematic of an experimental set-up, analysis of pattern uniformity and stability, and SERS application. See DOI: 10.1039/c9nr08056b

force, and Watson–Crick base pairing.[20,24–35] Among these, chemical patterning, in particular, shows great promise with robust and controllable substrate–particle interaction, and applicability to a range of different sizes and types of particles. To fabricate the patterns, a variety of techniques based on electron-beams,[36–38] scanning probes,[39–42] nanoimprinting, self-assembly of block copolymer films,[43–46] laser induced patterning[47,48] and electrohydrodynamic jet printing[49–52] have been used to date. These techniques have drawbacks in terms of throughput, cost, the need for specialized equipment, and the requirement of multi-step processing. These limitations strongly motivate the development of new fabrication approaches to direct the self-assembly of NCs.

As a low-cost, versatile and practical technique, electrospinning is a highly attractive approach to fabricate nanostructures. Previous studies have shown promise in the use of electrospun nanofibers (NFs) as templates for the directed assembly of nanostructures: intrinsically random NFs could be aligned and positioned to defined locations through near field electrospinning (NFES) aided by the rapid movement of the substrates.[53] These efforts either relied on the direct use[54–58] of NFs for decoration with nanostructures or employed NFs as masks[59–64] for selective material removal. The presence of NFs in the former approach can lead to issues in terms of the chemical and physical instability of the patterned arrays of NCs, whereas the latter subtractive approach challenges the fabrication of multiplex patterns and preservation of the intrinsic properties of the underlying substrate. An ideal approach should allow for the additive fabrication of covalently bound and ultrathin interfaces patterned within areas spatially defined by the NFs.

Here, we present a purely additive and versatile chemical patterning approach to directly fabricate nanoscale patterns with end-functional polymers from reservoirs that are confined within electrospun NFs. In this approach, end-functional polymers serve as inks to generate nanoscale patterns of end-grafted polymers on the substrate surface. The localized grafting of polymers in nanoscale dimensions is achieved *via* the confinement of the inks (functionalized polymers) within NFs that act like an inkpot. The width of the fabricated patterns is not only defined by the diameter of NFs, but also by the extent of spreading during the thermal annealing step, which is necessary for grafting polymers onto the substrate. Through tuning the kinetics of thermal annealing and by reducing the surface energy of the substrate, we demonstrate the fabrication of ultrathin (height < 15 nm) linear nanoribbons of poly(ethylene glycol) and poly(2-vinylpyridine) with sub-100 nm widths. The additive nature of our approach allows for the fabrication of multiple chemical patterns on the same substrate by sequential writing of different inks. The high-quality fabrication of nanoscale chemical patterns enables the directed assembly of various colloidal NCs without altering their properties, in a universal approach, including noble metal nanoparticles (Au, Ag, Pt), metal oxide nanoparticles (TiO_2), and semiconductor quantum dots (QDs) and 2D nanoplatelets.

Experimental

Writing patterns of ink-containing nanofibers

Solutions of poly(ethylene oxide) (PEO, 300.0 kg mol^{-1}, Sigma Aldrich) with hydroxyl-terminated poly(ethylene glycol) (PEG, 35.0 kg mol^{-1} Sigma Aldrich) (PEO/PEG) were prepared in water at a total concentration of 5% w/w (concentration of PEG is 35% w/w with respect to PEO). Solutions of 3% w/w poly(2-vinylpyridine) (P2VP, 200–400.0 kg mol^{-1} Poly Science) with 6.25% w/w hydroxyl-terminated poly(2-vinylpyridine) (P2VP, 22.8 kg mol^{-1}, PDI = 1.09 Polymer Source) and 0.3% w/w/poly(ethylene oxide) (PEO, 4000.0 kg mol^{-1} Sigma Aldrich), (P2VP-PEO/P2VP·OH) were prepared in 7/3 v/v *N*,*N*-dimethylformamide (DMF, Sigma Aldrich)/dichloromethane (DCM, Sigma Aldrich). The solutions were mixed with a magnetic stirrer at 700 rpm for ~6 h to ensure complete dissolution of the polymers. Electrospun NFs were directly written on bare, hydrophilic and hydrophobic silicon substrates (⟨100⟩ Wafer World Inc.). The bare silicon substrates were cleaned by washing in isopropanol and ethanol for 3 min under sonication, respectively. The hydrophilic substrates were prepared by 15 min UV-ozone cleaning treatment. The hydrophobic substrates were prepared by vapor-phase deposition of tridecafluoro-1,1,2,2-tetrahydrooctyl-trichlorosilane for 15 s. Spatially defined deposition of NFs was performed using near-field electrospinning assisted with an automated stage (see Fig. S1† for a schematic and photograph of the experimental set-up). The solutions were placed in a 2.5 mL syringe fitted with a blunt end 30 g metallic needle (outer diameter = 310 μm, inner diameter = 160 μm). The syringe was placed in a holder with a horizontal configuration against a programmable x–y stage (Parker MX80L). The silicon substrates were mounted on top of the stage with the aid of a vacuum suction. The tip-to-substrate distance was set as 1 to 2 mm and the feed rate of the solution varied from 0.5 μL h^{-1} to 2 μL h^{-1}. The potential between the needle and substrate was set between 500–750 V. The stage moved at a speed of 100 mm s^{-1} for the alignment of the fibers.

Localized grafting of end-functional polymers

The polymer solutions containing the end-functional polymers were electrospun onto the silicon substrates followed by annealing in an argon-filled glove box using a hot-plate. Upon annealing, the end-functional polymers within the electrospun NFs were grafted onto the substrates. To graft PEG·OH, annealing was performed at temperatures of 90 °C, 120 °C, 150 °C, and 180 °C for 3 min each. In the case of P2VP·OH, annealing was done at 200 °C for 3 min. The unbound end-functional polymers and the main NF materials (PEO for PEG and P2VP/PEO for P2VP·OH) were then removed by sonication in water for PEG and in DMF for P2VP, respectively. The sonication was repeated three times for 3 min each. The substrates were then blow-dried with nitrogen.

Site specific assembly of NCs on patterned nanoribbons

Citrate stabilized spherical gold NCs were immobilized on top of the patterned nanoribbons by placing a droplet of the sus-

pension of particles for 1 h, followed by washing in water under sonication for 2 min and drying with nitrogen. Other NCs were immobilized on grafted P2VP·OH nanoribbons using a similar procedure to that described above except with an immobilization time of 2 h.

Characterization

The surface morphology of the substrates was imaged with SEM (Zeiss EVO LS10) at 25 kV and focused ion beam SEM (FEI Nova NanoLab 600i) at 15 kV. The height profiles of the NFs after electrospinning, annealing, and washing were analyzed with AFM (Veeco Multimode 8). The freshly synthesized Ag nanocubes and CdSe/CdZnS semiconductor NCs were imaged with FEI Tecnai G2 F20 S-TWIN HR(S) TEM at 200 kV. The water contact angle of the substrate was analyzed using a contact-angle meter (Attension). The fluorescence microscopy images were taken using a fluorescence microscope (Olympus BX43, 488 nm single band) using an exposure time of 100 ms.

Results and discussion

Fig. 1a–f schematically show direct grafting of nanoscale patterns of functional polymers for guided assembly of colloidal NCs. In this process, end-functional polymers act as inks. NFs serve as reservoirs of these inks in an analogy with an inkpot. In this unique approach, inks are written in areas that are defined by the nanoscale inkpots presented by NFs. The process starts with electrospinning of highly aligned NFs in spatially defined positions. The alignment of NFs is accomplished by operating in the near field electrospinning (NFES) mode where the distance between the tip of the nozzle and substrate is less than 1 cm. The controlled and rapid movement of the substrate allows for precise control over the position of the NFs. In contrast to the previous reports,[54–64] NFs are employed as nanoscale reservoirs for end-functional polymers. The process of writing is achieved *via* a brief thermal annealing, which results in grafting of the end-functional polymers onto the substrate surface whose width is constrained by the diameter of the NF. The nanoscale chemical patterns that are defined with this localized grafting process are revealed by washing of the fiber and excess materials in a good solvent (water for PEG and DMF for P2VP). The fabricated nanoscale chemical patterns then serve as a template for directed assembly of a variety of colloidal NCs.

We first demonstrate directed assembly of Au NCs on nanoscale patterns of PEG. For this purpose, we prepared electrospun NFs using PEO that was blended with hydroxyl terminated PEG ink. The choice of PEO as the inkpot stems from several reasons. First, aqueous solutions of high molecular weight PEO with concentrations between 2–6% are highly suitable for fabricating highly aligned NFs using NFES, thanks to the viscoelastic characteristics of the polymer.[53,61,62,65] Second, having identical chemistry with low molecular weight PEG, the PEO inkpot is perfectly miscible with the ink. Note that insufficient levels of chain entanglement for the low molecular

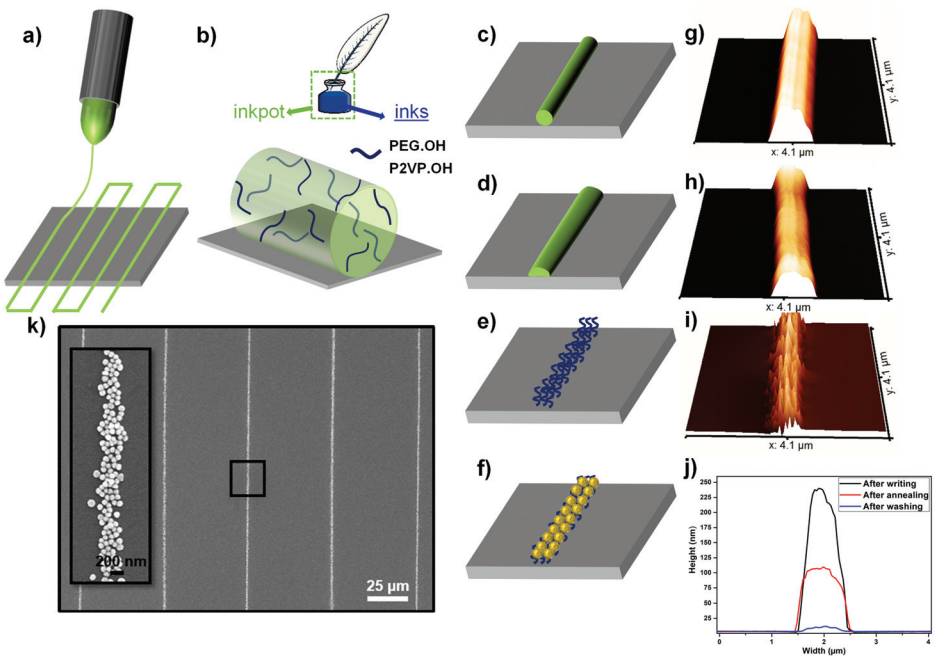

Fig. 1 Fabrication of spatially defined arrays of NCs. (a–f) Schematic illustration of the process. (a) Electrospinning of the solution containing end-functional polymers. (b) NFs as an inkpot containing end-functional polymers. (c–f) Depiction of a single NF after (c) writing, (d) annealing, (e) washing, and (f) immobilization of colloidal NCs. (g–i) AFM images of the electrospun NFs on the hydrophobized silicon substrate. (g) Pristine PEO/PEG NF, (h) after annealing, and (i) PEG nanoribbon after washing. (j) Height profiles of the patterns. (k) SEM images of the 60 nm Au NCs assembled on the grafted PEG nanoribbons with a pitch of ~50 μm.

weight PEG ink is not suitable for direct writing of NFs. Third, PEG proved to be highly effective for directing the assembly of Au NCs.[66–71] PEO NF inkpots were written on Si substrates through the control of the diameter between 100 nm and 550 nm *via* adjusting NFES parameters, such as voltage bias (500 to 750 V) and tip-to collector distance (1 to 2 mm). As a result of the annealing and washing processes (Fig. 1g–i), nanoribbons of grafted PEG patterns (Fig. 1e and i) were generated. The annealing of PEG results in the grafting of PEG·OH onto the Si substrate, through formation of an ester bond (Si–O–C) between the hydroxyl end of PEG and surface silanol group (Si–O–H) of the Si substrate.[66] After removing unreacted inks and the inkpot by washing, we generated PEG patterns with a height of ~10 nm (Fig. 1j), which is consistent with the ellipsometric thickness of the grafted PEG on the Si substrate.

We used spatially defined PEG nanoribbon patterns for selective assembly of citrate stabilized Au NCs (Fig. 1k). The selective binding of citrate-stabilized Au NCs to end-grafted PEG results in dense assembly of particles, revealing the chemical contrast of the patterns.[43] We found that three factors determine the final width of the nanoribbons and the density of immobilized NCs: (i) diameter of NF inkpots written by NFES, (ii) spreading behavior of the NF inkpot during thermal annealing, and (iii) kinetics of grafting. The spreading of the NF inkpot strongly depends on the surface energy of the substrate while the ink grafting ability strongly depends on the annealing temperature.

To investigate the effect of the aforementioned factors, we wrote NFs of a range of different diameters on bare, hydrophobized and freshly cleaned silicon substrates. To make the surface hydrophobic, the silicon substrate was treated with fluoroalkyl silane (FAS), namely tridecafluoro-1,1,2,2-tetrahydrooctyl-trichlorosilane *via* vapor-phase deposition.[72] For the freshly cleaned surface, the substrate was treated in a UV-ozone chamber to increase the hydrophilicity. We confirmed the extent of modification by measuring the water contact angles (see ESI Fig. S2b†) of the bare silicon substrate (50°), FAS deposited surface (110°), and the UV-ozone treated surface (20°).

The localized grafting of PEG inks onto the above-mentioned surfaces was then achieved *via* thermal annealing. The results are summarized in Fig. 2. Overall, there is noticeable spreading after annealing, resulting in the formation of chemi-

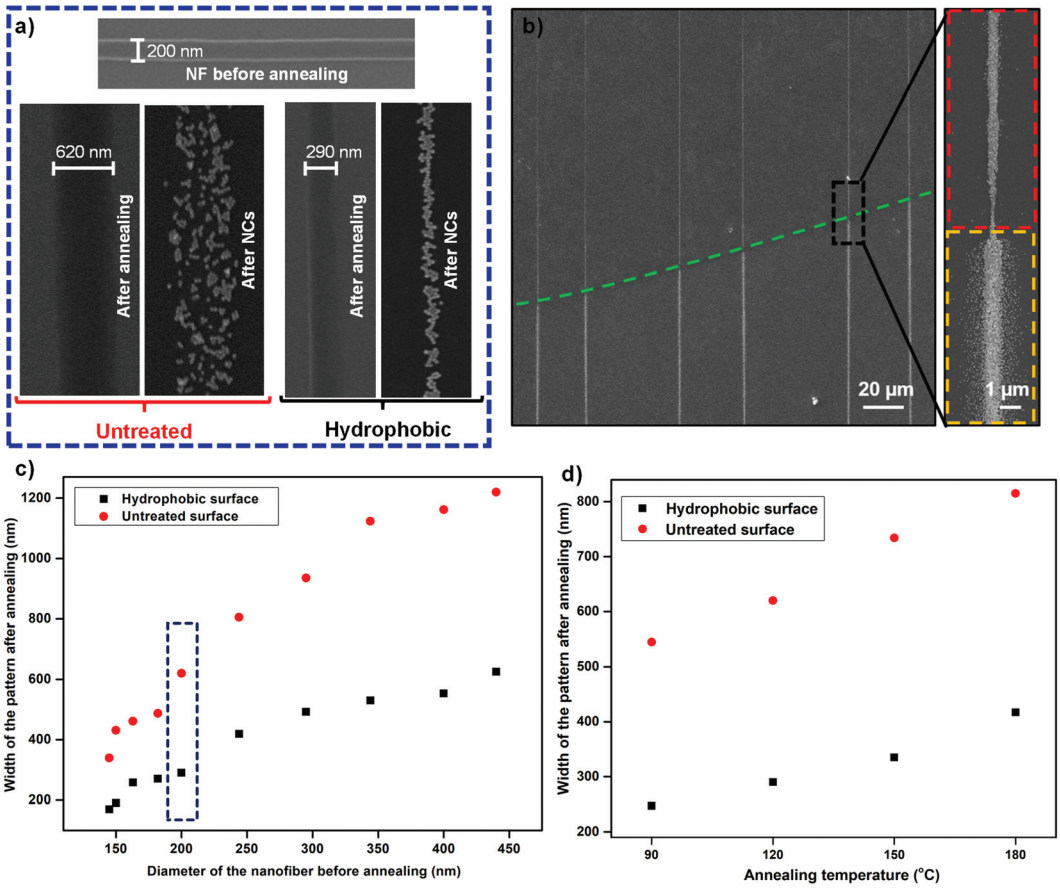

Fig. 2 (a) SEM images of the PEO inkpot, after annealing at 120 °C, and after immobilization of 40 nm Au NCs. (b) SEM image of nanoribbons decorated with 40 nm Au NCs, the dashed green line marks the borderline between the hydrophobic (top) and hydrophilic part (bottom) of the modified substrate. Also shown is a high magnification SEM image of a single nanoribbon where the boundaries between untreated and hydrophobized regions of the substrates are seen. (c) The width of the patterns as a function of the diameter of NF after annealing at 120 °C. (d) The effect of the annealing temperature on the spreading of a NF with a diameter of 200 nm on untreated and hydrophobized substrates.

cal patterns that are wider than the original NF inkpot. The selective binding of Au NCs in the fabricated nanoribbons after washing of excess materials reveals the dimension of the fabricated chemical patterns. The extent of spreading strongly depends on the surface of the substrate and annealing temperature, as can be clearly seen from Fig. 2a and Fig. S2 (ESI†). For example, upon annealing at 120 °C, a 200 nm diameter NFs spread to 620 nm on the bare substrate while on the FAS treated surface it is only 290 nm. To clearly demonstrate the impact of the surface of the substrate on the extent of spreading, we prepared a substrate where a segment was FAS derivatized to be hydrophobic and the remaining part was UV-ozone treated to be hydrophilic. The contrast of spreading is clearly visible along the boundary (Fig. 2b).

The diameter of the NF is critically important in determining the final width of the patterns. Fig. 2c presents the width of the patterns as a function of the diameter of NFs. The width of the pattern clearly scaled with the diameter of the fiber. For the entire range of NF diameters, the modification of the substrate with FAS suppressed the spreading, particularly for NFs with small diameters. The dependence of the spreading on the fiber diameter is likely a result of the length of the fiber–substrate interface.[61]

The grafting of PEG onto the substrate surface requires annealing which inadvertently causes spreading that must be minimized. As inferred from Fig. 2c & d, and Fig. S3 & Table S2,† the NF spreading increases as the annealing temperature increases. The ratios of the width of nanoribbons on a bare substrate to that of FAS treated hydrophobic surface are 2.08 ± 0.2, 2.00 ± 0.15, 1.85 ± 0.11, and 1.65 ± 0.46 for annealing temperatures of 90 °C, 120 °C, 150 °C and 180 °C, respectively (ESI Table S2†). We postulate that the decreasing ability of FAS to suppress spreading as temperature increases is likely due to the fact that the surface tension of liquids generally decreases as a function of temperature, completely disappearing at the critical temperature of the liquid.

The hydrophobicity of the substrate plays an important role in fabricating nanoscale patterns using the approach introduced here. The patterns generated on the FAS treated hydrophobic surface are not only narrow but also well-defined with clear boundaries and reduced line edge roughness. On the other hand, the spreading caused by the necessary annealing step also results in blurry boundaries that lead to visibly scattered Au NC dots upon immobilization. A comparison of Au NC immobilization onto PEG on the UV-ozone treated hydrophilic surface and the FAS treated hydrophobic surface clearly reveals the spreading and scattering upon annealing (Fig. S2†).

The results indicate that by adjusting the annealing temperature and modifying the substrate surface with low surface energy molecules, patterns at higher resolution can be fabricated. Another important factor that needs to be considered is the temperature dependent grafting ability of PEG which enables the immobilization of Au NCs. Even though the spreading is the least at 90 °C, the grafting density of PEG is low as indicated by the sparse immobilization of Au NCs (Fig. S2†). At temperatures above 120 °C, the binding of Au NCs onto the grafted PEG does not show a noticeable increase whereas the spreading is significant. Thus, we choose the annealing temperature as 120 °C for the hydrophobic surface, considering both the high immobilization density and high pattern resolution. Under these conditions, the patterns were highly uniform as derived from image analysis (see ESI, Fig. S4†). The SEM images taken from 40 different locations of a 1 cm long pattern fabricated using a NF inkpot with a diameter of 200 nm showed that the average width was 292 nm with a standard deviation of 23 nm. The analysis of an array of 50 lines resulted in the average width of 287 nm with a standard deviation of 45 nm.

The treatment of Si substrate with FAS to make it hydrophobic greatly suppresses the spreading which results in the binding of an increased number of Au NCs upon immobilization. This gives us great flexibility to tune the generated patterns. Fig. 3 shows the SEM images of the patterns generated by the immobilization of Au NCs on grafted PEG. First, as shown in Fig. 3a, we immobilized Au NCs of 80 nm diameter on the nanoribbons of grafted PEG pattern of varying widths, from ~1100 nm (leftmost) to ~100 nm (rightmost). We found that the density of surface bound Au NCs increases slightly as the width of the PEG nanoribbon gets smaller. We further investigated the effect of the diameter of Au NCs on the assembly

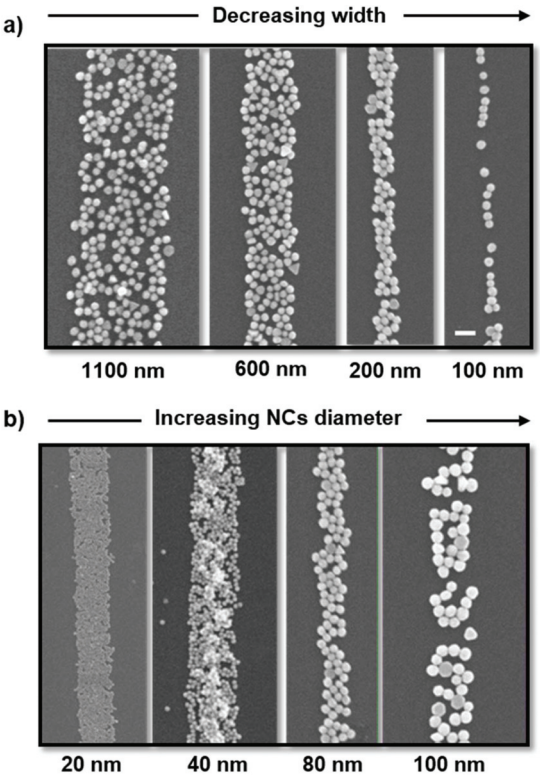

Fig. 3 SEM images of the (a) Au NCs (80 nm) immobilized on the patterns of grafted PEG nanoribbons of various widths (scale bar is 200 nm), and (b) Au NCs with various diameters immobilized on the patterns of grafted PEG nanoribbons of ~400 nm width. The width of nanoribbons (a) and sizes of Au NCs (b) are indicated at the bottom of the corresponding images.

process (Fig. 3b). The immobilization density of small NCs is large, but NCs as large as 100 nm can be also successfully immobilized with relatively high density. The density of surface bound Au NCs is higher on the PEG nanoribbons than the values reported for the unpatterned substrates that were modified with a layer of end-grafted PEG.[62,68] We believe that the localized grafting from the nanoscale inkpot, along with the suppressed spreading achieved by hydrophobic surface modification, enabled the dense immobilization of Au NCs. The seed-mediated growth[73] of metallic structures over patterned Au NCs of small (<~30 nm) diameter can enable the fabrication of continuous electrically conductive nanoscale patterns for transparent electrode applications.

An important aspect of the fabricated patterns is their robustness. For all the results presented in this study, the patterned substrates were washed under sonication following the grafting and immobilization of NCs. The high-density assembly of NCs within patterned regions indicates strong substrate–polymer and NC–polymer interactions. To further probe the adhesion strength of the patterns, we performed an adhesive tape test on the patterns following the immobilization of NCs on both hydrophilic and hydrophobic substrates. The morphology of the patterns and density of the bound NCs remained mostly the same following the adhesive tape test on both types of substrates (ESI, Fig. S6†). These results collectively suggest the robust assembly of NCs on patterned features.

One potential application of the fabricated patterns is in molecular sensing through surface-enhanced Raman spectroscopy (SERS). The assembly of spherical gold NCs into dense and close-packed structures within linear features results in a significant enhancement of Raman signals due to the formation of plasmonic hotspots where electromagnetic fields are focused in between nanoparticles that are separated by few nanometres of distance. Fig. S5† shows the SERS mapping results of a probe molecule on the patterns fabricated by localized grafting of PEG chains.

Assembly of colloidal NCs of varying compositions and geometries

We have demonstrated that PEG can be grafted at the nanoscale (as low as 50 nm) with well-defined boundaries resulting in highly selective and dense assembly of Au NCs. Despite the versatility of PEG in terms of fabricating nanoscale patterns and assembly of Au NCs, ink chemistry should be modulated to enable the assembly of a broad range of colloids on the patterns fabricated in this study. A highly suitable ink material is poly(2-vinylpyridine) (P2VP) with its reported high affinity to NCs of various compositions.[74–77] Hydroxyl-terminated P2VP can be grafted on the silicon substrates similar to PEG.[75–77]

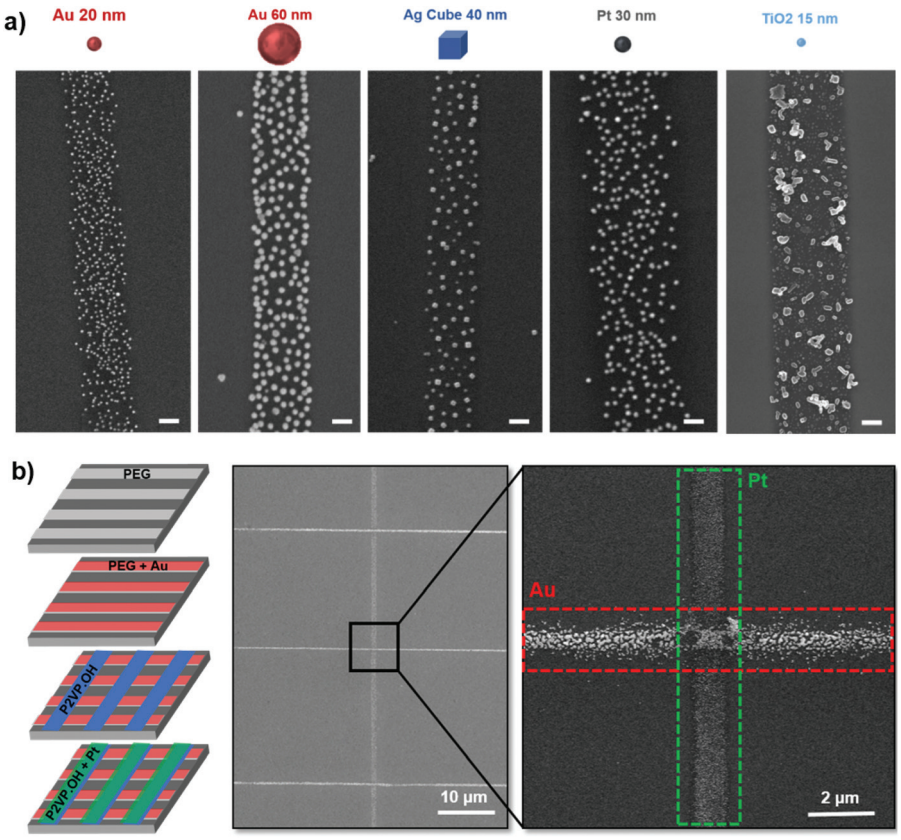

Fig. 4 Capabilities of the presented fabrication approach. (a) SEM images of the arrays of NCs of varying compositions, geometries and sizes on patterned nanoribbons of P2VP (scale bar is 200 nm), and (b) multiplex patterning. Schematic description and SEM images of the substrates that were patterned with PEG and P2VP nanoribbons following immobilization of Au and Pt NCs, respectively.

The relatively higher melting point of P2VP (>200 °C) in comparison with PEG (~65 °C) also informs about the impact of the mobility of the polymer ink on the spreading behavior during the grafting process.

P2VP inkpots on untreated Si substrates with controlled widths from 220 nm to 950 nm were achieved *via* adjusting the electrospinning parameters. Subsequent annealing at 200 °C followed by washing off the excess and unbound materials resulted in end-grafted P2VP nanoribbons with ~6 nm thickness (Fig. S7†), which is comparable to the results of previous studies on homogeneous substrates.[75,76] Upon annealing, the P2VP inkpot also spreads, though less than the PEO inkpot. For example, a 310 nm wide P2VP inkpot extends to a width of ~650 nm upon annealing at 200 °C while a 295 nm wide PEO inkpot spreads over ~940 nm upon annealing at 120 °C.

To demonstrate the versatility of the patterned P2VP nanoribbons, we generalized our findings by immobilizing NCs of metals, metal oxides, nanoplatelets and QDs. Due to the lone pair of electrons of the nitrogen in the pyridine group, it is expected that P2VP can bind to the NCs through electrostatic interactions and coordination bonds.[74] It is likely that long-range electrostatic interactions are important in the approach of the NCs to the substrate and short-range coordination bonds contribute to the strong binding, which can withstand washing under sonication. Commercially available spherical NCs of varying compositions (Au, Pt, TiO_2) could be directly assembled on the patterns without the need for any post-functionalization steps. Ag nanocubes were synthesized by the polyol method (see ESI & Fig. S9†). Fig. 4a shows the SEM images of immobilized NCs of various types and sizes on the patterned P2VP nanoribbons, clearly demonstrating the versatility of the P2VP nanoribbons for immobilizing various NCs.

The fabrication of multiple chemical patterns with different monotype or heterotype NCs precisely on the exact surface is a very hard task for even the most advanced nanolithography methods. To show the advantage of additive nature of our approach, we fabricated multiple chemical patterns on the same substrate by sequential writing of PEG and P2VP. First PEG with Au NCs were fabricated and then on the same surface P2VP patterns with Pt NCs were prepared as vertically intersecting the PEG patterns (Fig. 4b). The intersecting area of the patterns can exhibit multifunctional properties, for example, catalytic properties of Pt and plasmonic properties of Au.

To further demonstrate the versatility of our approach, we have further extended our study utilizing semiconductor colloidal quantum dots (QDs) and quantum wells that were immobilized on P2VP nanoribbons with a high yield (Fig. S8† and Fig. 5). Colloidal 2D nanocrystals, also named nanoplatelets (NPLs) or colloidal quantum wells, have emerged as a new material system within the quantum confined nanomaterial family. The NPLs possess dimensions on the order of tens of nanometers in the lateral direction along with precisely controlled vertical thickness, which would give flexibility in tuning their optical properties. Their giant absorption cross section

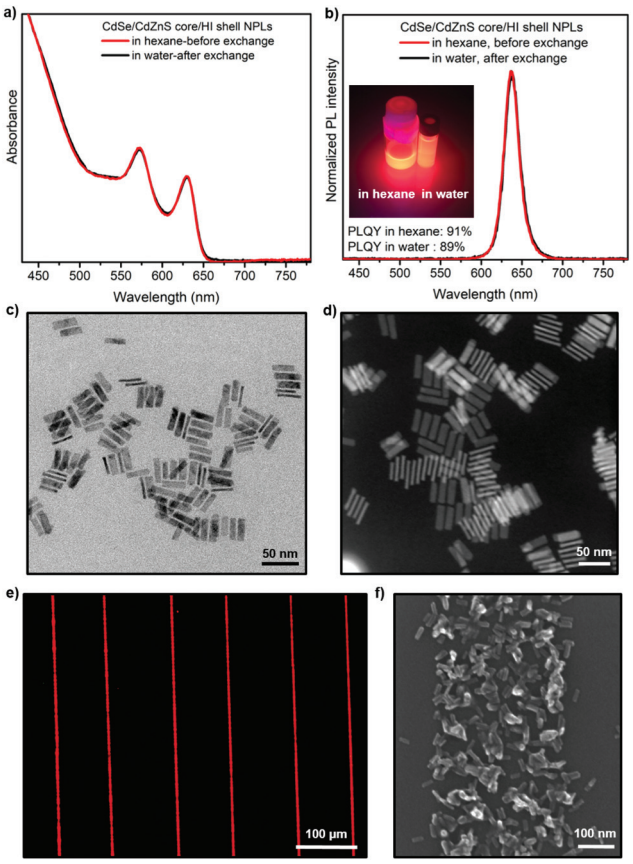

Fig. 5 (a) Absorbance, (b) photoluminescence spectra of CdSe/CdZnS core/HI shell NPLs before (in hexane) and after ligand exchange (in water). Inset shows a sample photograph under UV-illumination, (c) transmission electron microscopy, (d) high-angle annular dark-field scanning transmission electron microscopy (HAADF-STEM) images of CdSe/CdZnS core/HI shell NPLs, (e) fluorescence microscopy image of P2VP nanoribbons immobilized with CdSe/CdZnS core/HI shell NPLs, and (f) SEM image of P2VP nanoribbons following immobilization of CdSe/CdZnS core/HI shell NPLs.

and high spectral purity make these NPLs important building blocks for the next generation colloidal optoelectronics.

Here, we synthesized high quality and environmentally stable CdSe/CdZnS core/shell NPLs by using a hot-injection (HI) shell growth technique.[78] Then, we efficiently used a ligand-exchange procedure to make NPLs soluble in water (see the ESI†). Photoluminescence (PL) and absorption spectra of the NPLs before and after ligand exchange are given in Fig. 5a and b. The peak emission wavelength, full-width at half-maximum (FWHM) and quantum yield (QY) of the synthesized NPLs in the organic phase are 637 nm, 22 nm and 91% respectively. After ligand exchange, the optical properties of the NPLs are fully preserved (Fig. 5a and b). No spectral red shift, broadening of FWHM or a significant decrease in PLQY is observed in PL spectra and absolute QY measurements as given in Table S1.† The length, width and thickness of the NPLs are 36 ± 3 nm, 10 ± 1 nm and 3.9 ± 0.3 nm measured using TEM images presented in Fig. 5c and d. These high-quality emitters enable us to obtain bright and localized emis-

sion in the fluorescence microscopy image (Fig. 5e) and also show dense and selective immobilization of the particles as shown in Fig. 5f.

We also demonstrate spherical CdSe/ZnS QDs in the water phase that can be effectively immobilized on P2VP patterns along with their material characterization results provided in Fig. S8.† The patterning of these highly emissive QDs and NPLs on a predefined substrate is critical in order to warrant the spatial arrangement of the particles that are believed to open up new possibilities for LEDs and laser applications integrating patterned nanostructures.

Conclusion

This study has presented a unique utilization of electrospun NFs in fabricating nanoscale patterns for the assembly of inorganic NCs including colloidal metal, metal oxide nanoparticles, semiconductor QDs and NPLs. The nanoscale confinement of covalently bound ultrathin interfaces in areas defined by NFs offers a universal approach for the patterning of inorganic nanoscale building blocks in an unprecedented way. The strength of this approach stems from the additive patterning of NCs over large-areas using an inexpensive, reproducible, versatile nano-manufacturing based on electrohydrodynamic processes which could open up new possibilities in the industrial adoption of the proposed patterning technique. The resulting patterns offer exciting avenues of research in areas that range from patterning of the nano–bio assemblies to the fabrication of invisible nanoscale electrodes for applications in electronics.

Conflicts of interest

There are no conflicts to declare.

Acknowledgements

This work was supported by TUBITAK under Grant No. 115M517. M. S. O. and E. M. acknowledge support from the Turkish Academy of Sciences Distinguished Young Scientist Award (TUBA-GEBIP). ICN2 is supported by the Severo Ochoa program from Spanish MINECO (Grant No. SEV-2017-0706) and is funded by the CERCA Programme Generalitat de Catalunya. H. V. D. gratefully acknowledges TUBA.

Notes and references

1 M. A. Boles, D. Ying, T. Hyeon and D. V. Talapin, *Nat. Mater.*, 2016, **15**, 141.
2 E. Roduner, *Chem. Soc. Rev.*, 2006, **15**, 583.
3 K. L. Kelly, E. Coronado, L. L. Zhao and G. C. J. Schatz, *Chem. B*, 2003, **107**, 668.
4 E. Ozbay, *Science*, 2016, **311**, 389.
5 N. Wu, *Nanoscale*, 2018, **10**, 2679.
6 V. Reboud, G. Leveque, M. Striccoli, T. Placido, A. Panniello, M. L. Curri, J. A. Alducin, T. Kehoe, N. Kehagias, D. Mecerreyes, S. B. Newcomb, D. Iacopino, G. Redmond and C. M. S. Torres, *Nanoscale*, 2013, **5**, 239.
7 A. Genc, J. Patarroyo, J. Sancho-Parramon, N. G. Bastus, V. Puntes and J. Arbiol, *Nanophotonics*, 2013, **6**, 193.
8 M. Layani, A. Kamyshny and S. Magdassi, *Nanoscale*, 2014, **6**, 5581.
9 D. Wang, Y. Mei and G. Huang, *J. Semicond.*, 2018, **39**, 110021.
10 D. Chen, Z. Liu, B. Liang, X. Wang and G. Shen, *Nanoscale*, 2012, **4**, 3001.
11 Y. Liu, K. Zhang, W. Li, J. Ma and G. J. Vancso, *J. Mater. Chem. A*, 2018, **6**, 7741.
12 Y. Wu, D. Wang and Y. Li, *Chem. Soc. Rev.*, 2014, **43**, 2112.
13 A. Ruditskiy, H.-C. Peng and Y. Xia, *Annu. Rev. Chem. Biomol. Eng.*, 2016, **7**, 327.
14 A. T. Bell, *Science*, 2003, **299**, 1688.
15 A. Llordes, G. Garcia, J. Gazquez and D. J. Milliron, *Nature*, 2013, **500**, 323.
16 J. Piella, F. Merkoci, A. Genc, J. Arbiol, N. G. Bastus and V. Puntes, *J. Mater. Chem. A*, 2017, **5**, 11917.
17 S. J. Tan, M. J. Campolongo, D. Luo and W. L. Cheng, *Nat. Nanotechnol.*, 2011, **6**, 268.
18 V. F. Puntes, K. M. Krishnan and A. P. Alivisatos, *Science*, 2001, **291**, 2115.
19 J. Patarroyo, A. Genc, J. Arbiol, N. G. Bastus and V. Puntes, *Chem. Commun.*, 2016, **52**, 10960.
20 P. Alivisatos, P. F. Barbara, A. W. Castleman, J. Chang, D. A. Dixon, M. L. Klein, G. L. McLendon, J. S. Miller, M. A. Ratner, P. J. Rossky, S. I. Stupp and M. E. Thompson, *Adv. Mater.*, 1998, **10**, 1297.
21 S. J. Koh, *Nanoscale Res. Lett.*, 2007, **2**, 519.
22 H. Zeng, J. Li, J. P. Liu, Z. L. Wang and S. H. Sun, *Nature*, 2002, **420**, 395.
23 V. F. Puntes, P. Gorostiza, D. M. Aruguete, N. G. Bastus and A. P. Alivisatos, *Nat. Mater.*, 2004, **3**, 263.
24 L. Chen, B. Su and L. Jiang, *Chem. Soc. Rev.*, 2019, **48**, 8.
25 M. Grzelczak, J. Vermant, E. M. Furst and L. M. Liz-Marzan, *ACS Nano*, 2010, **4**, 3591.
26 L. C. Ma, R. Subramania, H. W. Huang, V. Ray, C. U. Kim and S. J. Koh, *Nano Lett.*, 2007, **7**, 439.
27 M. Jiang, J. A. Kurvits, Y. Lu, A. V. Nurmikko and R. Zia, *Nano Lett.*, 2015, **15**, 5010.
28 Y. Ofir, B. Samantha, Q. Xiao, B. J. Jordan, H. Xu, P. Arumugam, R. Arvizo, M. T. Tuominen and V. M. Rotello, *Adv. Mater.*, 2008, **20**, 2561.
29 E. Palleau, N. M. Sangeetha, G. Viau, J.-D. Marty and L. Ressier, *ACS Nano*, 2011, **5**, 4228.
30 S. Kralj and D. Makovec, *ACS Nano*, 2015, **9**, 9700.
31 B. Bharti, A.-L. Fameau and O. D. Velev, *Faraday Discuss.*, 2015, **181**, 437.
32 Y. Cui, M. T. Björk, J. A. Liddle, C. Sönnichsen, B. Boussert and A. P. Alivisatos, *Nano Lett.*, 2004, **4**, 1093.
33 C. Lalander, Y. Zheng, S. Dhuey, S. Cabrini and U. Bach, *ACS Nano*, 2010, **4**, 6153.

34 M. S. Onses, P. Pathak, C. C. Liu, F. Cerrina and P. F. Nealey, *ACS Nano*, 2011, **5**, 7899.
35 A. M. Hıng, C. M. Micheel, L. D. Bozzano, L. W. Osterbur, G. M. Wallraff and J. N. Cha, *Nat. Nanotechnol.*, 2010, **5**, 121.
36 P. A. Schaal, A. Besmehn, E. Maynicke, M. Noyong, B. Beschoten and U. Simon, *Langmuir*, 2012, **28**, 2448.
37 R. Nidetz and J. Kim, *Nanotechnology*, 2012, **23**, 045602.
38 U. C. Coskun, H. Mebrahtu, P. B. Huang, J. Huang, D. Sebba, A. Biasco, A. Makarovski, A. Lazarides, T. H. LaBean and G. Finkelstein, *Appl. Phys. Lett.*, 2008, **93**, 123101.
39 S. Kramer, R. R. Fuierer and C. B. Gorman, *Chem. Rev.*, 2003, **103**, 4367.
40 X. Liu, Y. Li and Z. Zheng, *Nanoscale*, 2010, **2**, 2614.
41 Z. Xie, C. J. Chen, X. C. Zhou, T. T. Gao, D. Q. Liu, Q. Miao and Z. J. Zheng, *ACS Appl. Mater. Interfaces*, 2014, **6**, 11955.
42 W. M. Wang, R. M. Stoltenberg, S. Liu and Z. Bao, *ACS Nano*, 2008, **2**, 2135.
43 M. S. Onses, C.-C. Liu, C. J. Thode and P. F. Nealey, *Langmuir*, 2012, **28**, 7299.
44 S. S. Kim and B. H. Sohn, *RSC Adv.*, 2016, **6**, 41331.
45 M. J. Pavan and R. Shenhar, *J. Mater. Chem.*, 2011, **21**, 2028.
46 M. S. Onses, L. Wan, X. Y. Liu, N. B. Kiremitler, H. Yılmaz and P. F. Nealey, *ACS Macro Lett.*, 2015, **4**, 1356.
47 B. Kang, J. Kim and M. Yang, *Opt. Express*, 2012, **20**, 29111.
48 J. Kim, S. G. Kwon, S. Back and B. Kang, *Appl. Surf. Sci.*, 2018, **434**, 693.
49 M. S. Onses, E. Sutantoi, P. M. Ferreira, A. G. Alleyne and J. A. Rogers, *Small*, 2015, **11**, 4237.
50 B. F. Porter, N. Mkhize and H. Bhaskaran, *Microsyst. Nanoeng.*, 2017, **3**, 1.
51 Y. Altintas, I. Torun, A. F. Yazici, E. Beskazak, T. Erdem, M. S. Onses and E. Mutlugun, *Chem. Eng. J.*, 2020, **380**, 122493.
52 J. Schneider, P. Rohner, P. Galliker, S. N. Raja, Y. Pan, M. K. Tiwari and D. Poulikakos, *Nanoscale*, 2015, **7**, 9510.
53 D. Sun, C. Chang, S. Li and L. Lin, *Nano Lett.*, 2006, **6**, 839.
54 W. Kim, J. S. Lee, D. H. Shin and P. Jang, *J. Mater. Chem. B*, 2018, **6**, 1272.
55 W. Tang, D. B. Chase and J. F. Rabolt, *Anal. Chem.*, 2013, **85**, 10702.
56 S. Patel and G. Hota, *RSC Adv.*, 2016, **6**, 15402.
57 L. Zhang, X. Gong, Y. Bao, Y. Zhao, M. Xi, C. Jiang and H. Fong, *Langmuir*, 2012, **28**, 14433.
58 R. S. Gill, R. F. Saraf and S. Kundu, *ACS Appl. Mater. Interfaces*, 2013, **5**, 9949.
59 S.-Y. Min, Y. Lee, S. H. Kim, C. Park and T.-W. Lee, *ACS Nano*, 2017, **11**, 3681.
60 H. Cho, S.-H. Jeong, S.-Y. Min, T.-H. Han, M.-H. Park, Y.-H. Kim, W. Xu and T.-W. Lee, *Adv. Opt. Mater.*, 2016, **4**, 967.
61 N. B. Kiremitler, S. Pekdemir, J. Patarroyo, S. Karabel, I. Torun, V. F. Puntes and M. S. Onses, *ACS Macro Lett.*, 2017, **6**, 603.
62 S. Karabel Ocal, J. Patarroyo, N. B. Kiremitler, S. Pekdemir, V. F. Puntes and M. S. Onses, *J. Colloid Interface Sci.*, 2018, **532**, 449.
63 Z. Ye, A. S. Nain and B. Behkam, *Nanoscale*, 2016, **8**, 12780.
64 T. He, A. Xie, D. H. Reneker and Y. A. Zhu, *ACS Nano*, 2014, **8**, 4782.
65 Y. A. Huang, Y. Duan, Y. Ding, N. Bu, Y. Pan, N. Lu and Z. Yin, *Sci. Rep.*, 2014, **4**, 5949.
66 N. A. Alcantar, E. S. Aydil and J. N. Israelachvili, *J. Biomed. Mater. Res.*, 2000, **51**, 343.
67 S. Pekdemir, S. Karabel, N. B. Kiremitler, X. Liu, P. Nealey and M. S. Onses, *ChemPhysChem*, 2017, **18**, 2114.
68 S. K. Ocal, S. Pekdemir, M. Serhatlioglu, H. H. İpekci, E. Sahmetlioglu, I. Narin, F. Duman, C. Elbuken, G. Demirel and M. S. Onses, *ACS Sustainable Chem. Eng.*, 2019, **7**, 4315.
69 M. S. Onses and P. F. Nealey, *Small*, 2013, **9**, 4168.
70 A. Karatay, B. Kucukoz, S. Pekdemir, M. S. Onses and A. Elmali, *Opt. Mater.*, 2017, **73**, 83.
71 M. S. Onses, *Langmuir*, 2015, **31**, 1225.
72 I. Torun, Y. Altintas, A. F. Yazici, E. Mutlugun and M. S. Onses, *ACS Appl. Nano Mater.*, 2019, **2**, 1185.
73 M. Sakir, S. Pekdemir, A. Karatay, B. Küçüköz, H. H. Ipekci, A. Elmali, G. Demirel and M. S. Onses, *ACS Appl. Mater. Interfaces*, 2017, **9**, 39795.
74 S. Malynych, I. Luzinov and G. Chumanov, *J. Phys. Chem. B*, 2002, **106**, 1280.
75 I. Tokareva, S. Minko, J. H. Fendler and E. Hutter, *J. Am. Chem. Soc.*, 2004, **126**, 15950.
76 H. Yilmaz, S. Pekdemir, H. H. Ipekci, N. B. Kiremitler, M. Hancer and M. S. Onses, *Appl. Surf. Sci.*, 2016, **385**, 299.
77 I. Torun, N. Celik, M. Hancer, F. Es, C. Emir, R. I. Turan and M. S. Onses, *Macromolecules*, 2018, **51**, 10011.
78 Y. Altintas, K. Gungor, U. Quliyeva, O. Erdem, Y. Kelestemur, E. Mutlugun, M. V. Kovalenko and H. V. Demir, *Small*, 2019, **15**, 1804854.